Journal of Theoretical and Applied Mechanics, Sofia, Vol.54 (2024) pp. 405-428
SPECIAL ISSUE

# APPLICATION OF DIFFERENT MODELLING TECHNIQUES FOR SOIL-STRUCTURE INTERACTION PROBLEMS IN ANISOTROPIC MEDIA

SONIA PARVANOVA[1]*, GEORGI VASILEV[1], AMAR PASHOV[2]

[1]*Department of Structural Engineering, University of Architecture, Civil Engineering and Geodesy, Sofia, Bulgaria*
[2]*KU Leuven, Department of Civil Engineering, Kasteelpark Arenberg 40, B-3001 Leuven, Belgium*

[Received: 30 September 2024. Accepted: 13 December 2024]

**doi: https://doi.org/10.55787/jtams.24.54.4.405**

ABSTRACT:

The current paper investigates wave propagation from time-harmonic embedded point source in a semi-infinite anisotropic medium containing underground structure by applying three different computational techniques. Firstly, direct BEM for 2D elastodynamics is applied using the fundamental solution derived by the Radon transform for general anisotropic continua. The second numerical technique is a computationally efficient two-and-a-half dimensional FEM, used to calculate the 3D wave field in the soil. At the boundaries of the mesh perfectly matched layers are instated to prevent spurious wave reflections. The FEM solutions realized by the built-in options in ANSYS are finally utilized with two types of absorbing boundary conditions. The results obtained by the three adopted modelling techniques are properly compared and respective insights regarding their applications are provided.

KEY WORDS: 2.5D elastodynamics; Anisotropic soil–tunnels interaction; BEM; FEM–PMLs; ANSYS.

## 1 INTRODUCTION

The main aim of the current study is to investigate the three-dimensional (3D) wavefield radiated by a thin circular lined tunnel embedded in an anisotropic half-space. The presence of infrastructures beneath the free surface of the ground lead to amplifications of surface motion and dynamic stress concentrations due to the wave scattering, wave diffraction and wave interference occurring between the stress-free ground and surfaces of the embedded structures when subjected to seismic waves or

*Corresponding author e-mail: slp_fce@uacg.bg

moving vehicles. The soil generally is anisotropic due to the long-term geological sedimentation processes in its formation. In the pioneering work of Stoneley [1] it was observed that the wave propagation in the medium is sensitive to soil anisotropy. State-of-the-art reviews regarding the wave propagation in anisotropic media are provided by Bramford & Crampin [2] and Crampin et al. [3]. The dynamic response of elastic and rigid circular plates embedded in viscoelastic, transversely isotropic (TI), three-dimensional layered media was presented by Labaki et al. [4]. More recently, the effects of anisotropic and poroelastic soil properties on the dynamic response of rigid circular foundations is presented in Keawsawasvong & Senjuntichai [5]. The current paper deals with the application of different numerical techniques for modeling anisotropic soil-tunnel interaction systems. The methods used in this study are applicable for general anisotropy, but our focus is on the TI and monoclinic materials to restrict the number of input parameters.

The main challenge in modeling of soil-structure interaction (SSI) systems is the infinite nature of the ground beneath the stress-free surface. The boundary element method (BEM) is a widespread technique for the analysis of wave scattering in elastodynamics because its formulation via boundary integral equations is equivalent to the original Boundary-Value Problem (BVP), described by partial differential equations. Its analytically derived fundamental solution ensures a high level of accuracy by satisfying Sommerfeld's radiation condition for waves traveling towards infinity. The finite element method (FEM) is currently the most popular and universal technique for numerical modelling with numerous applications. To circumvent the difficulty arising due to the semi-infinite nature of the half-space many artificial boundary conditions at the truncated boundary of the finite elastic domain are developed. In the current study we employ in the numerical modeling the abilities of perfectly matched layers (PMLs) and infinite finite elements (FE).

The application of BEM for anisotropic SSI problems is associated with the work of Gazetas [6], who presented a semi-analytical solution for dynamic responses of a rigid strip footing on an incompressible transversely isotropic soil stratum. The dynamic response of an arbitrary shaped rigid strip foundation embedded in an orthotropic elastic half-plane by indirect BEM was reported in Wang and Rajapakse [7]. A displacement-based BEM for a determination of the dynamic impedance functions of arbitrarily shaped, embedded strip foundations in inhomogeneous soil media could be found in Chatzistefanou and Manolis [8]. The 3D and two-dimensional (2D) time-domain elastodynamic fundamental solutions (Green's functions) for linearly elastic anisotropic materials are initially obtained by the Radon transform in Wang and Achenbach [9]. A comprehensive and extensive application of BEM in 2D elastodynamics for anisotropic media in frequency domain is provided by Garcia-Sanchez [10]. The scattering and diffraction of plane qP- and qSV-waves by a canyon

in a multi-layered TI half-space in both frequency and time domains was examined by Ba et al. [11]. Indirect BEM was used more recently by Ba *et al*. [12, 13] to study the dynamic impedance of rigid foundations embedded in anisotropic layered half-plane. Parvanova and Dineva [14] applied the direct BEM to solve a 2D dynamic problem in frequency and time domains for a flexible foundation of arbitrary geometry resting in an elastic anisotropic half-plane. Elastic wave scattering by cracks at macro- and nano-scale in anisotropic plane under plane-strain state was studied in Dineva and Rangelov [15] and Rangelov *et al*. [16]. Elastic time-harmonic and transient wave scattering by multiple anisotropic nanoiclusions in an infinite anisotropic medium under plane strain conditions are considered in Parvanova and Dineva [17].

The tunnels are structures of infinite length which are invariant in longitudinal direction. For such structures the solution could be performed for 2D geometry, even if the dynamic source remains 3D. Such solution is referred as two-and-a-half dimensional (2.5D) or quazi-3D approach where the 3D wave field in the soil-tunnel system is represented through 2D discretization in the wavenumber-frequency domain. The solution involves computing a sequence of 2D problems across a range of spatial wavenumbers. The spatial solution in the direction in which the geometry does not vary is then obtained by means of inverse Fourier transform. The 3D seismic response of 2D topographies using full-space Green's functions for a harmonic point force moving along a direction parallel to the generatrix of the topography was examined by Pedersen et al. [18] applying the indirect BEM. The 3D dynamic response of lined tunnels in a half-space by the BEM was evaluated in Stamos and Beskos [19]. By a coordinate transformation and appropriate integration of the full space dynamic fundamental solution, the problem was reduced to a 2D one along the direction of the tunnel axis. 2.5D Green's functions for 3D elastodynamic problems are presented in Tadeu and Kausel [20] derived by using integral transform methods and/or boundary elements. In Jean et al. [21] a 2.5D Green function for a given wave number along the infinite direction is provided. To investigate the dynamic interaction between layered soil and longitudinally invariant structures Francois et al. [22] developed a 2.5D coupled finite element–boundary element methodology. A BEM to calculate displacements in anisotropic layered soil caused by a vibrating load inside a tunnel was presented in Rieckh et al. [23] considering 2.5D problem. More recently, Liravi et al. [24] predicted the 3D wave field in longitudinally invariant soil-structure interaction problems by a 2.5D coupled FEM-BEM-Method of Fundamental Solutions (MFS) methodology. Modelling of 3D wave propagation in a layered TI medium with the Thin Layer Method (TLM) and complex frequency shifted PMLs could be found in Li *at al*. [25]. The authors observed that traditional PMLs applied with TLM may lead to exponentially increasing backpropagation waves, attributed to material anisotropy when simulating TI media.

To cope with the challenge of semi-infinite domains the built-in options in ANSYS propose infinite FE and PMLs. The PMLs as truncated boundary in the FEM was originally introduced for absorbing electromagnetic waves by Berenger [26] extended for structural elastodynamics by Basu and Chopra [27]. Placed next to the elastic finite domain the PML absorbs nearly perfectly all mechanical waves traveling towards infinity without any reflections from the contact interface between the elastic region and the layer. There are some reflected waves from the fixed outer boundary of the absorbing layer, but it could be made as small as desired (ANSYS [28]). A single layer of infinite elements can represent an exterior subdomain of infinite regions in FEM based software ANSYS. This approach is applicable to static and both harmonic and transient analyses, although in the current ANSYS release it is considered only the case of elastic isotropic material.

The core numerical technique employed in the current study is a 2.5D FEM-PMLs formulation proposed originally by Francois *et al*. [29], derived in a weak form for an isotropic medium. In order to adjust the 2.5D FE mesh, at first comparisons are performed with BEM solutions for 2D plane-strain state problems. Then for verification purposes, FEM solutions are carried out using the built-in options of ANSYS for both isotropic and anisotropic mediums. Furthermore, three types of problem dimensionality are examined: 2D plane-strain case by BEM, 2.5D FE-PMLs which can be applied for plane-strain state and 3D wave propagation problems, and finally 3D FEM by ANSYS software package. In sum, two numerical methods BEM and FEM are employed in the present numerical simulations, and three types of infinite boundaries are applied: global natural infinite boundary by BEM, and two artificial truncated boundaries by FEM – infinite FE and PMLs. All the obtained results are properly compared and verified.

The paper is organized as follows: The problem statement together with its reformulation via boundary integral equations and via FEM combined with PMLs are given in Section 2. What follows is the verification of the developed computational scheme in Section 3 along with the respective numerical results, illustrating the effects of the soil anisotropy. Finally, the concluding remarks are summarized in Section 4.

## 2 Problem Outline

### 2.1 Boundary value problem

The wavefield radiated by an underground tunnel $\Omega_{\mathrm{t}}$ embedded in an anisotropic halfspace $\Omega_{\mathrm{hs}}$ in a Cartesian Coordinate System (CCS) $Ox_1x_2x_3$ due to a unit vertical harmonic point load is the problem under consideration. The tunnel structure is invariant of infinite size along $Ox_2$ axis (See Fig. 1a).

The governing equation of motion in frequency domain is expressed as

$$\sigma_{ij,j}(\mathbf{x},\omega) + \rho\omega^2 u_i(\mathbf{x},\omega) = f_{0i}\delta(\mathbf{x},\mathbf{x}_0,\omega), \quad \mathbf{x}(x_1,x_2,x_3) \in \Omega_{\text{hs}},\Omega_{\text{t}}\,. \tag{1}$$

Here $\sigma_{ij}$ are the stress components; $\mathbf{x}\,(x_1,x_2,x_3)$ is the position vector of the observer point; $\rho$ is the mass density; $u_i\,(\mathbf{x},\omega)$, $i = 1,2,3$ are displacement components, related with the strain tensor $\varepsilon_{ij}$ by the geometry equation $\varepsilon_{ij} = (u_{i,j} + u_{j,i})$, $i,j = 1,2,3$. Since the response is time-harmonic, the common multiplayer $\exp(\mathrm{i}\omega t)$ is suppressed. Comma subscripts denote partial differentiation with respect to the spatial coordinates, while the summation convention over repeated indices is implied.

The general form of the constitutive stress-strain equation is $\sigma_{ij} = C_{ijkl}\varepsilon_{kl}$, where $C_{ijkl}$ is the fourth-order stiffness tensor for elastic anisotropic continuum which contains 81 constants. Due to the symmetry of the stress and strain tensors, these constants are reduced to 21 independent parameters in case of general anisotropy. In what follows the contracted notations of Voigt are used for the stiffness tensor components.

TI materials are a special case of orthotropic materials which have three material planes of symmetry. Additionally TI materials have identical properties in horizontal $Ox_1x_2$ plane which reduces the independent stiffness tensor parameters to five: horizontal Young's modulus $E_h = E_1 = E_2$; vertical Young's modulus $E_v = E_3$; vertical shear modulus $G_v = c_{44} = c_{55}$; horizontal Poisson ratio $\nu_h = \nu_{12}$; vertical-horizontal Poisson's ratio $\nu_{vh} = \nu_{31} = \nu_{32}$. These parameters are related to $c_{11}$, $c_{13}$ and $c_{33}$ stiffness tensor components by the following expressions [13]:

$$\begin{aligned} c_{11} &= \frac{E_h\left(1 - \frac{E_h}{E_v}\nu_{vh}^2\right)}{(1+\nu_h)\,\bar{v}}\,; \qquad & c_{13} &= \frac{E_h\nu_{vh}}{\bar{v}}\,; \\ c_{33} &= \frac{E_h\,(1-\nu_h)}{\bar{v}}\,; & \bar{v} &= 1 - \nu_h - 2\frac{E_h}{E_v}\nu_{vh}^2\,. \end{aligned} \tag{2}$$

For the rest of the nonzero stiffness components in case of TI materials the following relations are truth: $c_{22} = c_{11}$, $c_{23} = c_{13}$ and $c_{12} = c_{11} - 2c_{66}$. The horizontal shear modulus is $c_{66} = E_h/\,(2\,(1+\nu_h))\,.$

The monoclinic materials are the second category of the anisotropic materials considered in the current paper. They have one plane of symmetry assumed here $Ox_1x_3$ normal to the longitudinal tunnel direction. The symmetric stress and strain components with respect to the plane of symmetry are $\sigma_{11}$, $\sigma_{22}$, $\sigma_{33}$, $\sigma_{13}$ and $\varepsilon_{11}$, $\varepsilon_{22}$, $\varepsilon_{33}$, $\varepsilon_{13}$ respectively. The anti-symmetric components are $\sigma_{12}$, $\sigma_{23}$ and $\varepsilon_{12}$, $\varepsilon_{23}$. This results in 13 independent parameters defining the monoclinic material stiffness tensor.

The boundary conditions along the free surface are tractions free. For the soil-tunnel interface the traction equilibrium and displacement compatibility are satisfied. Finally, the traction free boundary conditions are fulfilled along the internal tunnel wall interface.

### 2.2 BEM FORMULATION FOR 2D ANISOTROPIC CONTINUUM

For 2D problems in plane-strain state, a verified authors' BEM software is used, based on the frequency-dependent fundamental solution (FS) derived by Radon transform for 2D general anisotropic continua [14]. In this case the TI half-space in the $Ox_1x_2x_3$ CCS becomes half-plane in $Ox_1x_3$ plane with $x_2 = 0$. The mechanical model defined in frequency domain via governing Eq. (1) is numerically solved by the displacement-based BEM. The fundamental solution of the partial differential equation (1) in conjunction with the dynamic equivalent to Betti's reciprocity theorem lead to the following expression, see [30]:

$$C_{ij}u_j(\mathbf{x},\omega) = \int_{\Gamma_\Omega} U^*_{ij}(\mathbf{x},\xi,\omega)\, t_j(\xi,\omega)\, d\Gamma(\xi) - \int_{\Gamma_\Omega} T^*_{ij}(\mathbf{x},\xi,\omega)\, u_j(\xi,\omega)\, d\Gamma(\xi) + f_{0j}U^*_{ij}(\mathbf{x},\mathbf{x}_0,\omega), \tag{3}$$

In the above equation, the boundary $\Gamma_\Omega$ is the contour of the domain under consideration $\Omega_{\text{hs}}$ or $\Omega_{\text{t}}$, $C_{ij}$ is the jump term depending on the local geometry at the source (collocation) point $\mathbf{x} = (x_1, x_3)$, $\xi = (\xi_1, \xi_3)$ is the receiver (running) point; $U^*_{ij}$ and $T^*_{ij} = c_{ijql}U^*_{qk,l}n_k$ are the displacement and traction fundamental solutions, correspondingly, see Garcia-Sanchez [10]; $c_{ijql}$ is the stiffness tensor, $n_k$ is the outward pointing unit normal vector to the respective surface.

### 2.3 REFORMULATION OF THE POSED PROBLEM VIA FEM COMBINED WITH PMLS

In order to exploit the longitudinal invariance of the model, the wave field can be expanded into a Fourier series in $O\,x_2$ direction, reducing the computation to 2D numerical model at the same time calculating 3D response. This allows the soil-tunnel system to be represented through 2D discretization in the wavenumber-frequency domain applying a computationally efficient 2.5D approach. The original 3D problem is substituted by 2D mesh for each longitudinal wavenumber, $k_{x_2}$. The finite element used is 8-node isoparametric quadratic plane element with 3 nodal degrees of freedom, where the first two of them are conventional for plane-strain element. The third nodal degree of freedom is in longitudinal $Ox_2$ direction accounting for out-of-plane

wave transmission. To prevent spurious wave reflection at the boundaries of $\Omega_{\text{hs}}$ domain, PMLs are installed, see Fig. 2. The strain displacement relation in 2.5D context is:

$$\boldsymbol{\varepsilon} = \mathbf{B}_1 \mathbf{u}\left(x_2, \omega\right) + \mathbf{B}_2 \partial \mathbf{u}\left(x_2, \omega\right) / \partial x_2. \tag{4}$$

Here $\mathbf{u}\left(\mathbf{x}, \omega\right)$ is the nodal displacement vector of size 3. $\mathbf{B}_1$ and $\mathbf{B}_2$ are strain matrices, where the former is composed by operator which contains spatial derivatives in-plane of the model, the latter is related with out-of-plane spatial derivative, which is extracted from the differential operator as shown in eq. (4), see [29].

Applying a standard Galerkin procedure for solving partial differential equations (1) or virtual work principle, followed by a Fourier transform of the longitudinal coordinate $x_2$ to the longitudinal wavenumber $k_{x_2}$ the next system of equations is reached (See Francois et al. [29]):

$$\left(\mathbf{K}_0 - \omega^2 \mathbf{M} - \mathrm{i} k_{x_2} \mathbf{K}_1 - k_{x_2}^2 \mathbf{K}_2\right) \mathbf{d}\left(k_{x_2}, \omega\right) = \mathbf{F}\left(k_{x_2}, \omega\right). \tag{5}$$

In Eq. (5) $\mathbf{K}_0 = \sum \iint_A \lambda_1 \lambda_3 \mathbf{B}_1^{\mathrm{T}} \mathbf{C} \mathbf{B}_1 \mathrm{d}A$ represents the global stiffness matrix for a 2D in-plane problem, $A$ is the area of the particular finite element; $\mathbf{C}$ is the stiffness material tensor; $\mathbf{M} = \sum \iint_A \lambda_1 \lambda_3 \mathbf{N}^T \mathbf{N} \rho \, \mathrm{d}A$ is the mass matrix. Matrices $\mathbf{K}_1 = \sum \iint_A \lambda_1 \lambda_3 \left(\mathbf{B}_1^{\mathrm{T}} \mathbf{C} \mathbf{B}_2 - \mathbf{B}_2^{\mathrm{T}} \mathbf{C} \mathbf{B}_1\right) \mathrm{d}A$ and $\mathbf{K}_2 = \sum \iint_A \lambda_1 \lambda_3 \mathbf{B}_2^{\mathrm{T}} \mathbf{C} \mathbf{B}_2 \mathrm{d}A$ are global stiffness matrices responsible for 3D wave propagation combining both in-plane and out-of-plane wave motion; $\mathbf{d}$ is the global vector of nodal displacements, and $\mathbf{F}$ is the global load vector. The symbol $\sum$ in global stiffness matrices means sum over the finite elements. Finally, $\lambda_1$ and $\lambda_3$ are stretch functions attenuating propagating $(p)$ and evanescent $(e)$ waves, see Basu & Chopra [27]:

$$\lambda_i\left(s_i\right) = 1 + f_{s_i 0}^e \left(\frac{s_i}{L}\right)^m - \mathrm{i} \frac{f_{s_i 0}^p}{\alpha_0} \left(\frac{s_i}{L}\right)^m. \tag{6}$$

In Eq. (6) $L$ is the thickness of the PMLs, $s_i$, $i = 1, 3$ stands for the direction of the attenuated wave, $\alpha_0 = \omega L / C_{\text{S}}$ is a dimensionless frequency, $C_{\text{S}} = \sqrt{G_v / \rho}$ is the shear wave velocity. The attenuation coefficients $f_{s_i 0}^e$ and $f_{s_i 0}^p$ are chosen as proposed in Papadopoulos et al. [31]:

$$f_{s1 0}^p = f_{s3 0}^p = 20 \qquad \text{and} \qquad f_{s1 0}^e = f_{s3 0}^e = \frac{C_s \pi}{l_{\text{FE}} \omega} - 1, \tag{7}$$

where $l_{\text{FE}}$ is the size of the FE in the PMLs. The exponent $m$ is set to 2, as recommended in Basu & Chopra [27]. On the interface between the PMLs and the elastic domain the stretch functions have unit values, i.e. $s_i = 0$, $i = 1, 3$, see Fig. 2. We

note that for the elastic domain the same matrices are composed with $\lambda_1 = \lambda_3 = 1$. Based on the above formulation and constitutive relations in Section 2.1 a MATLAB [32] software code has been developed to handle the anisotropic soil-tunnel interaction problem.

### 2.4 Application of FEM software ANSYS for 3D wave propagation in soil-tunnel interaction system

Two types of artificial boundaries are incorporated in ANSYS [28] software package for modeling of a problem with an infinite open domain. These are structural infinite elements based on the theory of absorbing boundary for dynamic analysis, and PMLs for truncation of structural open domains. The infinite FE is applicable for static, time-harmonic and transient analyses but only isotropic material is allowed. The PMLs are restricted to static and time-harmonic analyses. Placed next to an elastic domain, PML absorbs nearly perfectly all waves traveling towards infinity which ensures the satisfaction of the Sommerfeld radiation condition. The amplitude of the reflected 1D wave is mathematically constrained through the following attenuation function $|A_R| = \exp\left(-2F\left(L\right)\right)$, where $F\left(L\right) = \int\limits_0^L f\left(x\right)\mathrm{d}x$, $x$ is the spatial dimension of propagation, $f\left(x\right) = f_0\left(x/L\right)^m$, $f_0$ is a constant which optimal value is automatically chosen by the program, the exponent $m$ is set to 2 by default. As before $L$ is the thickness of the PML. The attenuation decrement is controlled by the parameter $m$ and the thickness $L$, their increasing lead to faster attenuation of the reflected wave. The material of the FE in the PML zone could be anisotropic.

## 3 Numerical Results and Comparisons

### 3.1 Test example 1: A lined circular tunnel entirely embedded in an isotropic half-space under unit point load at the tunnel invert of magnitude $f_{0i}$, $i = 1, 2, 3$

The wavefield radiated by a thin circular lined tunnel embedded in an elastic isotropic half-space due to a unit vertical time-harmonic point load at the tunnel invert is the first numerical example. The center of the tunnel is located beneath the free surface at a 2 m depth. The external radius of the tunnel is 1 m, the tunnel wall thickness is 0.1 m, see Fig. 1a. The material properties of the soil are modulus of elasticity $E = 108$ MPa, Poisson's ratio $\nu = 1/3$, density $\rho = 1.8$ t/m$^3$. The hysteretic material damping in the soil medium is 5%. The tunnel wall has been ascribed a Young's modulus of 31000 MPa, Poisson's ratio of 0.2, density of 2.5 t/m$^3$, representing concrete, and hysteretic material damping 0.1%.

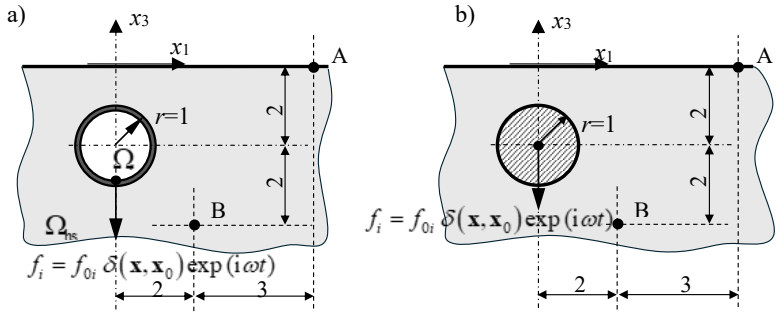


Fig. 1. Problem geometry: **a)** lined tunnel; **b)** cylindrical inclusion.

Following the solution of Liravi et al. [24] where the buried tunnel with the same mechanical properties was examined, at first the tunnel structure is replaced by a cylindrical inclusion. For verification purposes, the mechanical properties of the inclusion are identical with those of the surrounding soil reproducing an isotropic half-space. The problem geometry, the location of the observer points A and B, located at the stress-free ground surface and in the near field zone respectively, as well as the location of the force in the inclusion center, are indicated in Fig. 1b.

The current 2.5D FE-PMLs model solved by MATLAB code is shown in Fig. 2a. The FE mesh comprises 1237 quadratic quadrilateral 8 node FE with 3852 nodes. Symmetry is exploited to optimize the solution process. Half of the inclusion is discretized by 52 quadratic FE with 16 elements around the contact soil-inclusion interface. The PML thickness is equal to the inclusion radius, discretized by 5 FE in direction normal to the external boundary. The comparisons in the reference paper [24] are performed between displacement Green's functions for isotropic elastic

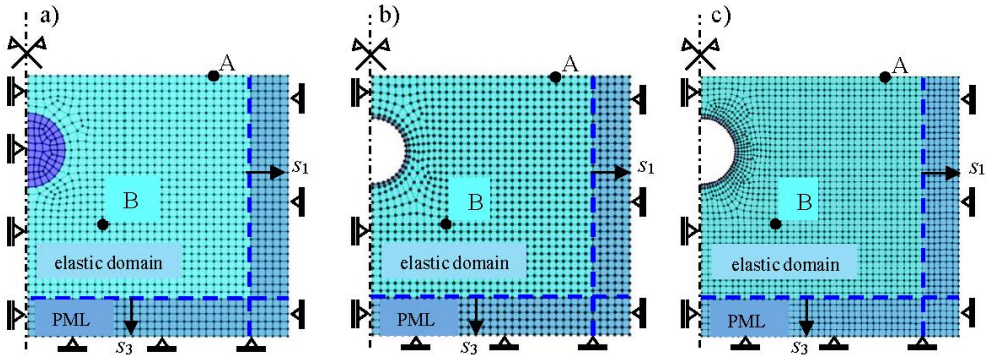


Fig. 2. FE-PMLs meshes: **a)** cylindrical inclusion; **b,c)** lined tunnel.

half-space, 2.5D BEM-FEM solution and 2.5D FEM-BEM-Method of Fundamental Solutions (MFS). The present results are compared with the displacement Green's functions in wavenumber frequency domain as reported in Liravi et al. [24] and perfect agreement with reference solution is observed. Due to a space limitation here only the last set of comparisons are reported in terms of receptance at both the observer points, presented in dB based on reference $10^{-9}$ m/kN. Due to the symmetry of the displacements caused by a unit point load in the wavenumber-frequency domain only the positive wavenumbers are considered in the current solution. The displacement components are transformed from wavenumber $k_{x_2}$ to space $x_2$ domain by inverse Fourier transform as follows:

$$u_i(x_2,\omega) = \frac{1}{\pi}\int_0^{\infty} u_i(k_{x_2},\omega)e^{-\mathrm{i}k_{x_2}x_2}dk_{x_2}, \tag{8}$$

where $i = 1, 3$ refers to the displacement component. To compute the desired receptance the wavenumber in the longitudinal direction is equally sampled from 0 to 55 rad/m into 257 points. The obtained receptance for both the representative points are shown in Fig. 3 together with the digitally captured results of Liravi et al. [24]. The frequency range of the results in the current modelling is 10-250 Hz with a step of 10 Hz.

What follows are comparisons for the buried tunnel structure. Two numerical models are considered in the present solution with relatively coarse and fine meshes. The coarse FE mesh comprises 1213 quadratic quadrilateral 8 node FE with 3792

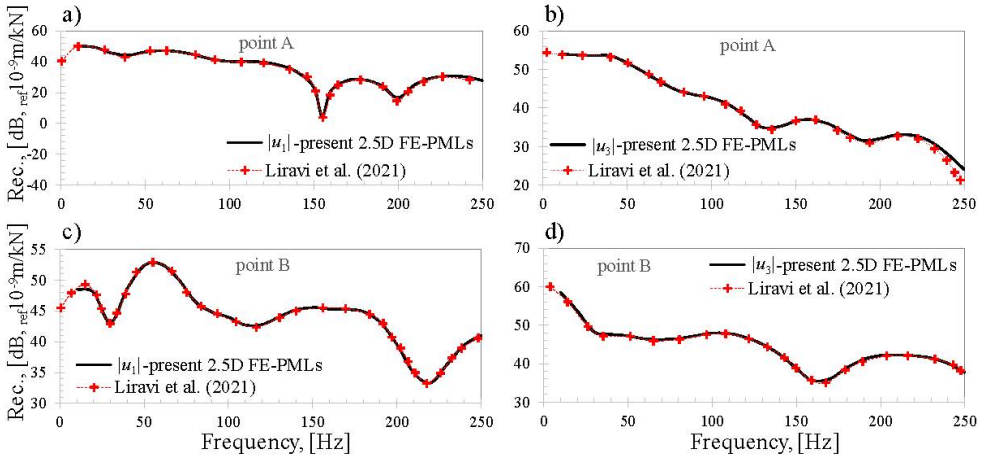


Fig. 3. Receptance versus frequency for the cylindrical inclusion model: **a**,**b)** point A with coordinates (5,0,0); **c**,**d)** point B with coordinates (2,0,-4).

joints. As before, symmetry is exploited to optimize the solution process. Half of the tunnel wall is discretized by 20 quadratic quadrilateral FE. The thickness of the PML strip is equal to the external radius of the tunnel $r = 1$ m, discretized by 5 FE in direction normal to the external boundary. The fine FE mesh consists of 1866 quadratic quadrilateral 8 node FE with 5797 joints. Half of the tunnel wall is discretized by 40 FE of the previous type. The unit thickness PML strip is discretized by 6 FE in the transverse direction. Both the meshes are depicted in Fig. 2b,c.

As before, the comparison is made in terms of receptance, presented in dB based on reference $10^{-9}$ m/kN, at the representative points. The wavenumber sampling in the current simulations is specified in terms of the dimensionless wavenumber $\bar{k}_{x_2} = k_{x_2} C_s/\omega$, where $C_s = \sqrt{\mu/\rho}$ is the SV-wave soil velocity, $\omega$ is the circular frequency, $\mu$ is the shear modulus of the soil. The dimensionless wavenumber is equally sampled from 0 to 3 into 301 points. The frequency range of the results in the current modelling is 5-250 Hz with a step of 5 Hz. The obtained receptance by both the FE meshes is shown in Fig. 4 together with the digitally captured results of Liravi et al. [24].

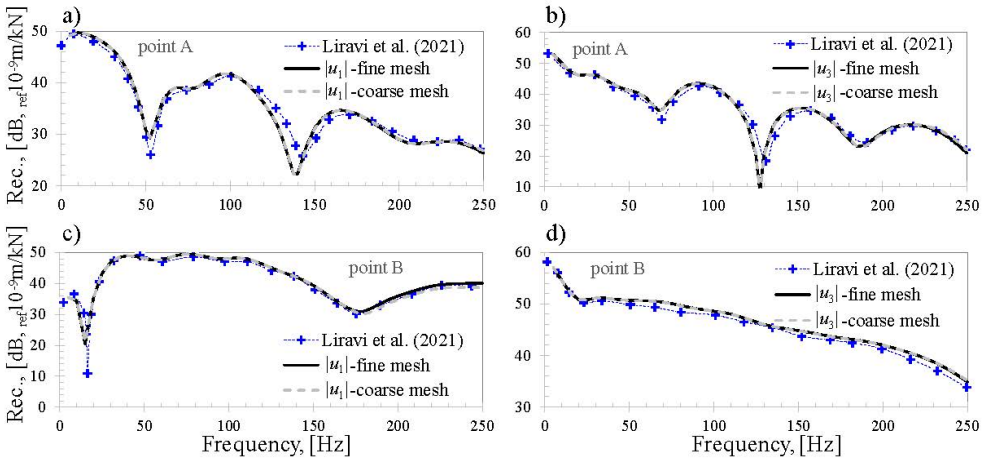


Fig. 4. Receptance versus frequency for the lined tunnel buried in isotropic half-space: **a**,**b)** point A with coordinates (5,0,0); **c**,**d)** point B with coordinates (2,0,-4).

### 3.2 Test example 2: A lined circular tunnel entirely embedded in TI half-space under a unit point load

The difference between the first test example and the current one is only in the characteristics of the half-space. Now it is transversely isotropic with prescribed ratio of the horizontal to vertical Young's modulus. In order to ensure positive diagonal

components of the material stiffness tensor, the denominator of eq. (2) should be positive:

$$\bar{\nu} = 1 - \nu_h - 2\frac{E_h}{E_v}\nu_{vh}^2 > 0 \qquad \Rightarrow \qquad \frac{E_h}{E_v} < \frac{1-\nu_h}{2\nu_{vh}^2} = 6\,, \tag{9}$$

which limits the variation of the elastic moduli ratio up to 6. This limitation implies the range of TI material types listed in Table 1 from $E_h/E_v = 0.1$ to $E_h/E_v = 5$. The vertical shear modulus of all material types is $G_v = 40500$ kN/m$^2$ the respective Poisson's ratios are $\nu_h = \nu_{vh} = 0.25$, the density is $\rho = 1.8$ t/m$^3$. The tunnel wall has the same mechanical properties as that in the first test example. The same is valid for the hysteretic damping ratio.

Table 1. Material properties

| Mat. type | Stiffness tensor components, [kN/m$^2$] | | | | | Elastic moduli, [kN/m$^2$] | |
|---|---|---|---|---|---|---|---|
| | $c_{11}$ | $c_{13}$ | $c_{33}$ | $c_{44}$ | $c_{66}$ | $E_h$ | $E_v$ |
| $E_h/E_v = 0.1$ | 19844.38 | 6240.37 | 187211.1 | 40500 | 7363.636 | 18409.09 | 184090.9 |
| $E_h/E_v = 0.25$ | 44373.91 | 14086.96 | 169043.48 | 40500 | 16200 | 40500 | 162000 |
| $E_h/E_v = 0.5$ | 76090.91 | 24545.45 | 147272.73 | 40500 | 27000 | 67500 | 135000 |
| $E_h/E_v = 1$ | 121500 | 40500 | 121500 | 40500 | 40500 | 101250 | 101250 |
| $E_h/E_v = 2$ | 189000 | 67500 | 101250 | 40500 | 54000 | 135000 | 67500 |
| $E_h/E_v = 4$ | 388800 | 162000 | 121500 | 40500 | 64800 | 162000 | 40500 |
| $E_h/E_v = 5$ | 742500 | 337500 | 202500 | 40500 | 67500 | 168750 | 33750 |

The first set of comparisons is between the solutions obtained by BEM and 2.5D FE approach combined with PMLs. Since the BEM is for 2D elastodynamics we consider plane strain state in $x_1x_3$ plane with $x_2 = 0$. In 2.5D FEM this is achieved by setting zero longitudinal wavenumber. The harmonic waves are radiated by a point source with coordinates (0,0,-0.8) located in the half-space domain in order to avoid the coincidence with a nodal point of the BE mesh in the BE model. The comparison is done for 4 materials with elastic moduli ratio 0.25, 0.5, 2, and 4.

The BEM mesh comprises 104 quadratic BE, 72 of which are used for the free surface of the half-plane discretizing length equal to +/-10$a$ with respect to the coordinate system origin. The cavity contour as well as each of the tunnel contours is modelled by 32 BE. The coarse FE mesh is exploited shown in Fig. 2b. The amplitudes of the normalized displacement components along the flat free surface versus space coordinate $x_1/r$ for two normalized frequencies $\Omega = \omega r/C_{\mathrm{S}} = 1$ and $\Omega = \omega r/C_{\mathrm{S}} = 2$ ($C_{\mathrm{S}} = \sqrt{G_v/\rho}$) for the four TI soil mediums are shown in Figs. 5 and 6. The results are in good agreement.

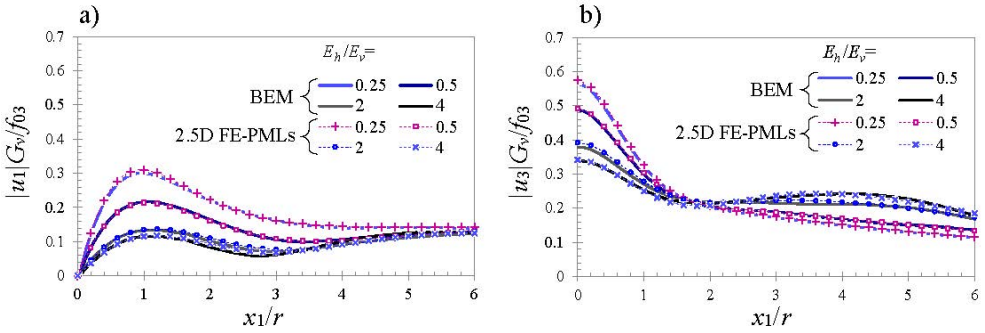


Fig. 5. Normalized displacements along the flat free surface for dimensionless frequency $\Omega = 1$, obtained by BEM and FE-PMLs for the 2D plane-strain case and different TI material types: **a)** horizontal components; **b)** vertical components.

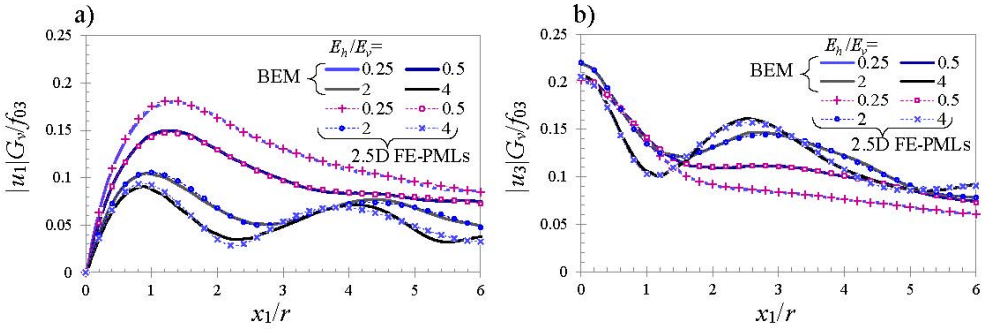


Fig. 6. Normalized displacements along the flat free surface for dimensionless frequency $\Omega = 2$, obtained by BEM and FE-PMLs for the 2D plane-strain case and different TI material types: **a)** horizontal components; **b)** vertical components.

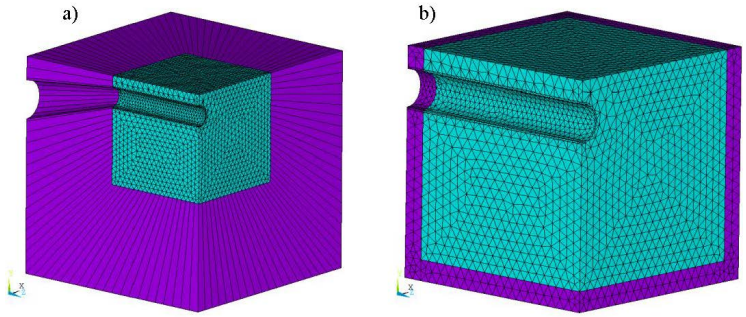


Fig. 7. 3D models in ANSYS **a)** with infinite FE; **b)** with PMLs.

The second set of comparisons concerns 2.5D FE-PMLs approach and 3D FEM solutions performed by ANSYS software. The point force is concentrated in the tunnel invert as depicted in Fig. 1a. As in the plane-strain case the coarse FE mesh is used for the 2.5D FE-PMLs modelling. Now this solution involves computing a sequence of 2D problems across a range of spatial wavenumbers defined in dimensionless form as $\bar{k}_{x_2} = k_{x_2} C_{\mathrm{S}}/\omega$. It ranges from 0 to 3, sampled with 301 equidistant points.

In 3D ANSYS solutions a quarter of the problem is modelled by applying appropriate boundary conditions at the planes of symmetry for better computational efficiency. In plane $(Ox_1x_3)$ and longitudinal ($x_2$ direction) size of the elastic domain is $10a$. For the TI soil types the 3D simulations are restricted to the use of PMLs as artificial boundaries, since the infinite FE are limited to isotropic materials. For the isotropic material type both the artificial boundaries are utilized. The volumetric finite elements used for the elastic domain discretization are specified as ten nodes quadratic SOOLID187 in ANSYS software. The respective infinite FE is INFIN257, the FE in the absorbing layer is SOOLID187 PML. Both the 3D FE meshes are depicted in Fig. 7. The first mesh associated with infinite FE comprises 2165 SOLID187 elements and 26 INFIN257 elements for the tunnel structure, and 67552 SOLID187 elements and 2672 INFIN257 elements for the half-space. The entire model consists of 105894 nodes with three nodal degrees of freedom (DOFs) which results in total number of 317682 DOFs (See Fig. 7a). The second FE mesh with PMLs comprises 2165 SOLID187 elements and 331 SOLID187 PML elements for the wall of the tunnel, and 67552 SOLID187 elements and 16127 SOLID187 PML elements for the half-space. Total number of nodes is 122280 with 366840 DOFs, see Fig. 7b.

The comparisons are performed based on the displacements in spatial coordinates for fixed frequency and for all material types listed in Table 1. The amplitudes of the vertical displacement components for the center point of the free surface or point with coordinates $(0, x_2, 0)$, and all material types for fixed frequency $f = 50$ Hz, are depicted in Fig. 8, as obtained by the 2.5D FE-PMLs approach and 3D ANSYS solution. The normalized horizontal displacement components along the free surface for the plane $x_2 = 0$ are presented in Fig. 9, and the vertical amplitudes of the surface displacements are portrayed in Fig. 10. The results are obtained by 2.5D FE-PMLs technique and FEM by built-in ANSYS options with PMLs as artificial boundaries for isotropic and TI soil materials and with infinite FE for isotropic soil mediums.

What follows is a short summary of the computational time required for the three numerical techniques. The 3D simulations were performed on a PC equipped with Intel Core i7-4790 CPU 3.6GHz, 4 cores. The computational time required by ANSYS software for the 3D model depicted in Fig. 7b with the results reported in Figs. 8–9

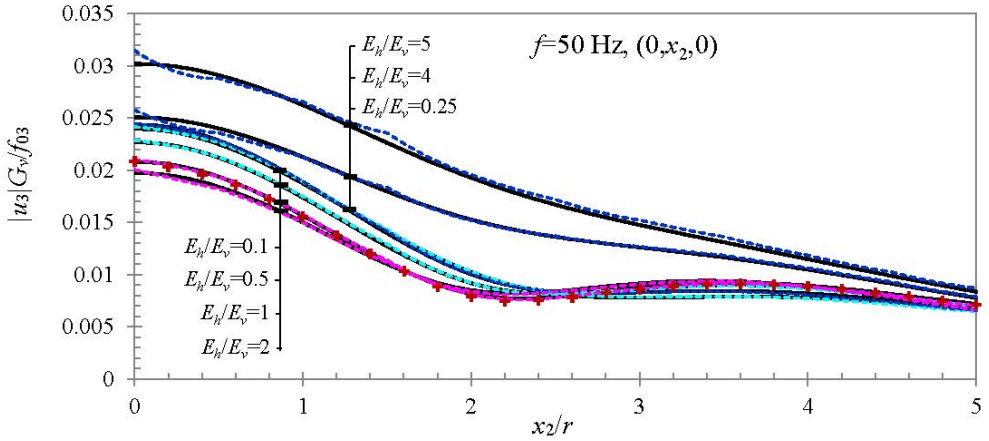


Fig. 8. Amplitudes of normalized vertical displacement components at the center point of the free surface along $x_2$ axis, for different TI soil types and fixed frequency $f = 50$ Hz, as obtained by the 2.5D FE-PMLs approach (black continuous lines) and the 3D ANSYS solution combined with PMLs (dashed lines). The red crosses plot is attained by 3D ANSYS solution with infinite FE for local artificial boundary.

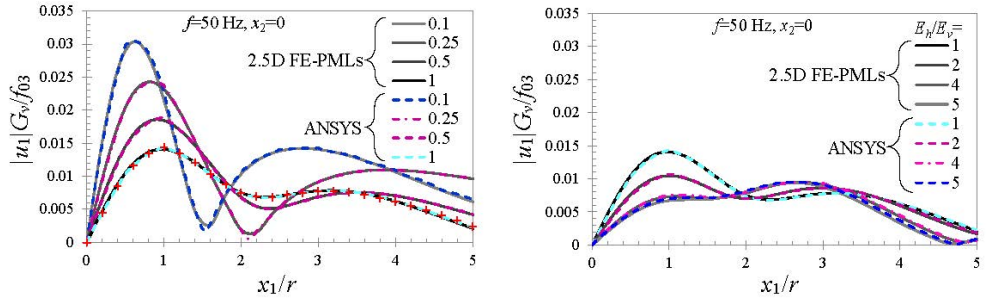


Fig. 9. Amplitudes of normalized horizontal displacement components at the free surface for $x_2 = 0$, for different TI soil types and fixed frequency $f = 50$ Hz. The red crosses plot is obtained by 3D ANSYS solution with infinite FE while dashed coloured lines are derived by 3D FEM combined with PMLs.

(element size 0.5 m) is 574 (s) for a single frequency. We note that the mesh depicted in Fig. 7b is the coarsest possible to recover the results reported in Figs. 8–9 for fixed frequency equal to 50 Hz. In order to get the same plotting accuracy for 100 Hz it is necessary to refine the 3D mesh, which we did not manage to achieve due to running out of RAM capacity of the PC used.

The MATLAB simulations were performed on a PC equipped with Intel(R) Core(TM) i7-4770 CPU 3.40GHz, 4 Core(s). The computational time required for

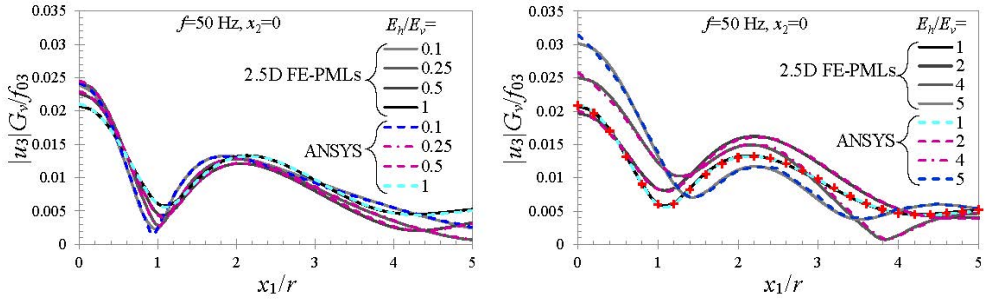


Fig. 10. Amplitudes of normalized vertical displacement components at the free surface for $x_2 = 0$, for different TI soil types and fixed frequency $f = 50$ Hz. The red crosses plot is obtained by 3D ANSYS solution with infinite FE while dashed coloured lines are derived by 3D FEM combined with PMLs.

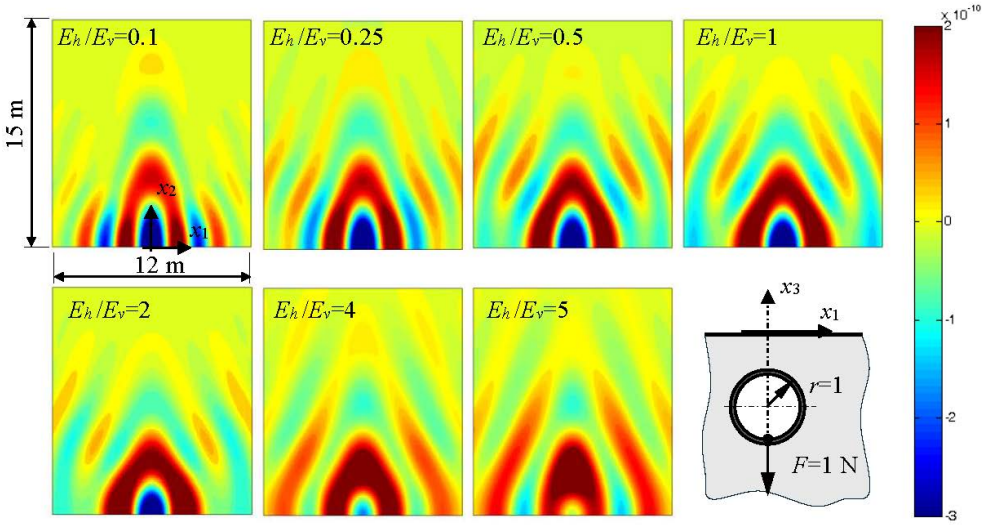


Fig. 11. Real part of the vertical displacement at the free surface due to a unit vertical point load at the tunnel invert at a frequency of 50 Hz.

the 2.5D FE-PMLs model depicted in Fig. 2b with the results reported in Figs. 5–6 and Figs. 8–9 (the coarse mesh with element size 0.2 m) is 7.8201 (s) for a fixed frequency and one wavenumber. The computational time for the BEM model with the results reported in Figs. 5–6 is 906.66 (s) for a single frequency (no wavenumber as the solution is 2D). The huge computational time of the BEM models is attributed to the fact that displacement fundamental solution for general anisotropic media requires not only standard integration over the line boundary element but also

the evaluation of a line integral over a unit circumference [10]. This double integration considerably slows down the solution process compared to the isotropic soil case.

The real part of the vertical displacement at the free surface due to a unit vertical point load at the tunnel invert and fixed frequency of 50 Hz are illustrated in Fig. 11 for all material types. Waves generated at the tunnel invert propagate through the TI soil and result in Rayleigh waves at the free surface. The influence of transverse

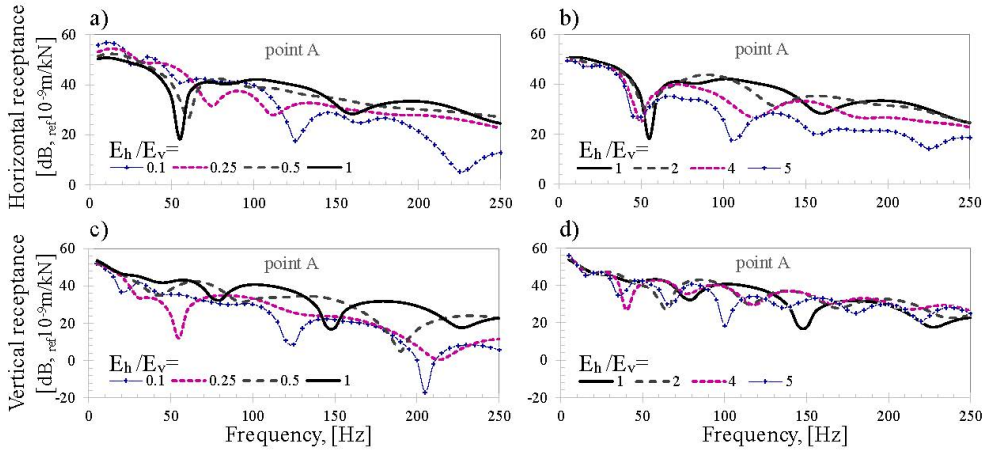


Fig. 12. Receptance versus frequency for point A and various TI material types: **a**,**b)** horizontal component; **c**,**d)** vertical component.

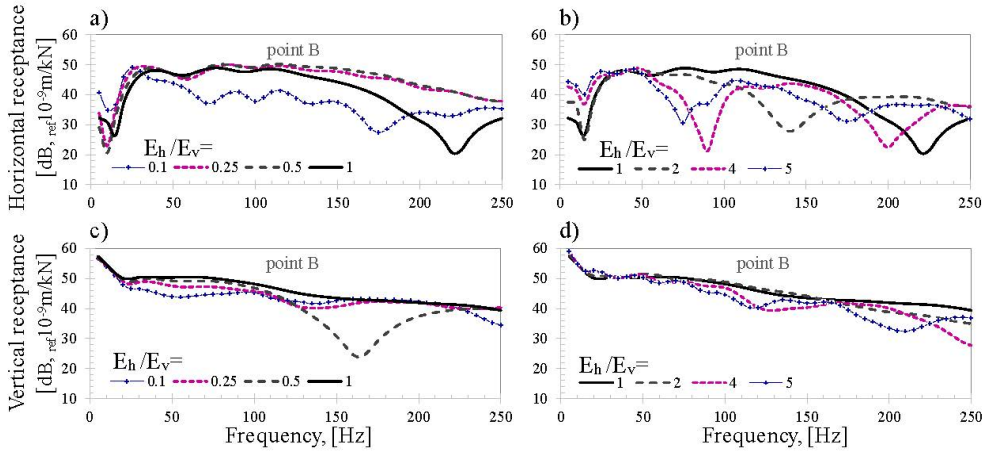


Fig. 13. Receptance versus frequency for point B and various TI material types: **a**,**b)** horizontal component; **c**,**d)** vertical component.

isotropy is clearly visible when compare with isotropic soil type. The dynamic interaction between the soil and the tunnel results in non-cylindrical wavefronts on the free surface.

Furthermore, the receptance of both the representative points A and B (See Fig. 1a) are now obtained for all the TI material types listed in Table 1. As before the receptance is presented in dB based on reference $10^{-9}$ m/kN. Amplitudes of horizontal and vertical displacements versus frequency at point A with coordinates (5,0,0) and at point B with coordinates (2,0,-4) for different material types are depicted in Figs. 12 and 13 respectively.

### 3.3 Test example 3: A lined circular tunnel entirely embedded in a monoclinic half-space under a unit point load

The last numerical example is the same lined tunnel described in Section 3.1 now embedded in a monoclinic half-space. Such materials have one plane of symmetry, assumed here parallel to $Ox_1x_3$ or normal to the longitudinal direction $Ox_2$. The constitutive stress-strain relation is adopted as follows:

$$(10)\quad \begin{Bmatrix} \sigma_{11} \\ \sigma_{22} \\ \sigma_{33} \\ \sigma_{12} \\ \sigma_{23} \\ \sigma_{31} \end{Bmatrix} = \begin{bmatrix} 184300 & 48300 & 23800 & 0 & 0 & -2000 \\ 48300 & 178400 & 21700 & 0 & 0 & 3900 \\ 23800 & 21700 & 59100 & 0 & 0 & 1200 \\ 0 & 0 & 0 & 72400 & 500 & 0 \\ 0 & 0 & 0 & 500 & 16000 & 0 \\ -2000 & 3900 & 1200 & 0 & 0 & 17600 \end{bmatrix} \begin{Bmatrix} \varepsilon_{11} \\ \varepsilon_{22} \\ \varepsilon_{33} \\ 2\varepsilon_{12} \\ 2\varepsilon_{23} \\ 2\varepsilon_{31} \end{Bmatrix}$$

The material stiffness matrix in Eq. (10) is derived from Bass (1995) for Muscovite. We note that stiffness matrix components in Eq. (10) have units kN/m$^2$ and they are 1000 smaller than those listed in Bass (1995) in order to have shear wave velocity similar to that in the first two examples. The density is assumed $\rho = 1.8$ t/m$^3$. Since the material is not symmetric with respect to the $Ox_2x_3$ plane, the plane-strain response of the soil-tunnel system is also non symmetric. Therefore, the whole in-plane model must be discretized or the meshes depicted in Fig. 2b, Fig. 2c, and Fig. 7 are not applicable for the current example. In that respect the 2.5D FE mesh comprises 2359 quadratic quadrilateral 8 node FE with 2484 joints. The tunnel wall is discretized by 40 quadratic quadrilateral FE. The PML thickness is equal to the external radius of the tunnel (1 m), discretized by 5 FE in direction normal to the external boundary.

As before, the first set of comparisons is between the 2D plane-strain solutions obtained by BEM and 2.5D FE approach combined with PMLs for zero longitudinal wavenumber. The harmonic waves are radiated by a point source with coordinates (0,0,-0.8) located in the half-space domain. The BE mesh is the same as that utilized

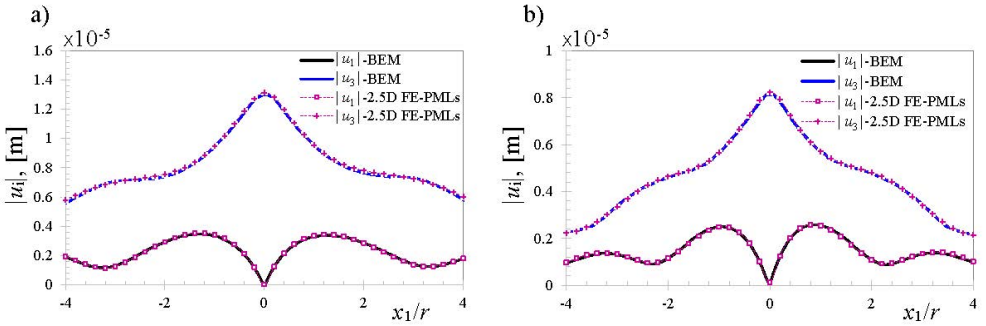


Fig. 14. Amplitudes of normalized displacement components along the free surface of a monoclinic soil medium for fixed normalized frequency $\Omega = \omega r/\sqrt{c_{55}/\rho}$: a) $\Omega = 1.52$; b) $\Omega = 3.03$.

in the second numerical example (Section 3.2). The amplitudes of the normalized displacement components along the flat free surface, as obtained by BEM and 2.5D FE-PMLs, for fixed normalized frequency $\Omega = \omega r/\sqrt{c_{55}/\rho}$ ($c_{55} = 17600$ kN/m$^2$) are depicted in Fig. 14. More specifically, in Fig. 14a $\Omega = 1.52$ and in Fig. 14b $\Omega = 3.03$. The results obtained by both numerical methods are nonsymmetric and almost identical.

The next set of comparisons is related to the results derived by 2.5D FE-PMLs and 3D ANSYS solutions. The unit point load is now concentrated at the tunnel invert. Half of the problem is modelled in 3D ANSYS solution by applying appropriate boundary conditions at the vertical plane of symmetry $Ox_1x_3$ with $x_2 = 0$ for better computational efficiency. The size of the discretized elastic domain is from -5$a$ to +5$a$ in $x_1$ direction, from 0 to 10$a$ in longitudinal $x_2$ direction and from 0 to -10$a$ in vertical $x_3$ direction. At the outer boundaries PMLs are installed. The FE mesh comprises 5579 SOLID187 elements and 745 SOLID187 PML elements for the wall of the tunnel, and 85929 SOLID187 elements and 20895 SOLID187 PML elements for the half-space. This results in total number of 162051 nodes with 486153 DOFs. The amplitudes of the vertical displacement components for the center point of the free surface or point with coordinates $(0, x_2, 0)$, for two fixed frequencies $f = 20$ Hz and $f = 40$ Hz, are depicted in Figs. 15a and 15c, respectively. The normalized horizontal displacement components along the free surface for the plane $x_2 = 0$ and the same normalized frequencies are portrayed in Figs. 15b and 15d, as obtained by the 2.5D FE-PMLs approach and 3D ANSYS solution. The wavenumber sampling in the current 2.5D FE-PMLs simulation is specified in terms of the dimensionless wavenumber $\bar{k}_y = k_y C_s/\omega$, where $C_s = \sqrt{c_{66}/\rho}$ is related to the horizontal $Ox_1x_2$ plane with $c_{66} = 72400$ kN/m$^2$. As before, the dimensionless wavenumber is equally

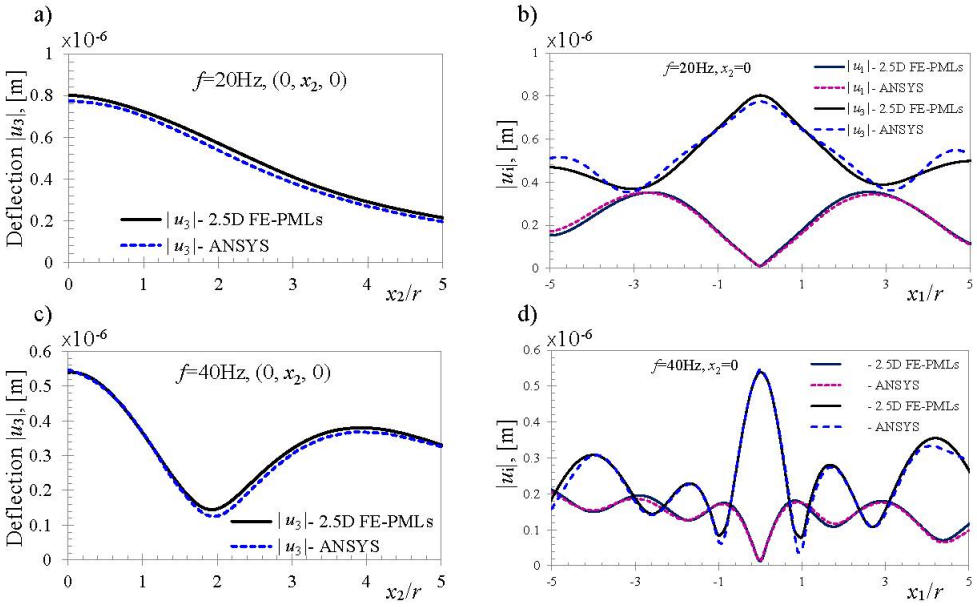


Fig. 15. Amplitudes of normalized displacement components of a monoclinic half-space for fixed frequency $f$ and: a),c) center point of the free surface with coordinates (0,$x_2$,0) along $x_2$ axis, b),d) free surface for $x_2 = 0$.

sampled from 0 to 3 into 301 points.

The good agreement between both sets of results observed in Figs. 14 and 15 proves that the 2.5 FE-PMLs methodology is not restricted only to TI or orthotropic mediums but is also applicable for more general case of monoclinic soils. We note that in the case of monoclinic material the response in longitudinal direction is still symmetric despite the lack of symmetry in the plane of the model. This allows us to consider only the positive wavenumbers like the previous examples. The discrepancies between both FE solutions observed in Fig. 15 are attributed to the relatively coarse FE mesh used in 3D ANSYS model, which cannot be refined due to running out of RAM capacity of the PC used.

## 4 Conclusions

A mechanical model for 3D elastic wave propagation in an anisotropic half-space containing lined tunnel and a point source of excitation is developed in this paper. The core numerical technique used for the numerical simulations is computationally efficient 2.5D FEM combined with PMLs accounting for the 3D wave propagation in general anisotropic continuum. The obtained results are first compared with existing

solutions in case of isotropic soil-tunnel system, then the outcomes for anisotropic media are confirmed by other numerical techniques. More specifically, the BEM is used to confirm the results in the case of 2D elastodynamics in plane-strain state. The good match between both sets of results proves the reliability of the 2.5D FE-PMLs technique in treatment of anisotropic domains since the BEM is considered as a semi-analytical approach. The 3D wave propagation in soil-tunnel system synthesized by applying 2.5D FE-PMLs methodology is verified by built-up options of commercial FE software ANSYS. In the latter method 3D models are considered and two types of artificial boundaries are employed: infinite FE in case of isotropic soil medium and PMLs for anisotropic material. The achieved good agreement between different sets of results proves that the solutions obtained by 2.5D FEM combined with PMLs are stable and accurate for a wide range of TI materials considered in the current study, since the elastic moduli ratio $E_h/E_v$ varies between 0.1 and 5. To expand the versatility of the 2.5D FE-PMLs approach beyond the simplification of TI soil medium, a comparison for tunnel structure embedded in a monoclinic half-space is performed. The respective results are non-symmetrical and in good agreement with the BEM solutions as well as with those derived by ANSYS software.

In sum, for 3D elastodynamics in anisotropic mediums the present 2.5 FEM-PMLs approach and built-in options of ANSYS with PMLs are applicable. The present 2.5D technique is more efficient in treatment of longitudinally invariant structures due to the reducing storage requirements with respect to the classical 3D solutions. Since 3D ANSYS solution is time-harmonic, the treatment of moving loads would be more complicated and requires longer discretization length in longitudinal direction which considerably increases the computational time and memory requirements. Contrary, the moving loads may be easily implemented in the soil-tunnel system in which the 3D wave field is obtained by 2D discretization in wavenumber-frequency domain in the framework of the 2.5D FEM.

The accuracy and potential of the 2.5 FEM-PMLs methodology has been successfully proven and verified by comparisons of the results published in the literature and by application of two different numerical methods, namely BEM and FEM. Furthermore, the versatility of this technique in modelling of different problem dimensionality is demonstrated. It represents 2D plane-strain case by setting zero wavenumber or 3D wave field can be synthesized by computing the problem across a range of spatial wavenumbers. Last but not least, the results obtained for the presented mechanical model and the wide range of TI materials as well as for the monoclinic soil medium, could serve as a benchmark example in the case of more complex models or application of other numerical techniques. To the best of authors' knowledge there is a lack of results considering the dynamic soil-tunnel interaction accounting for the material anisotropy and the current results contribute to fill this gap.

ACKNOWLEDGMENTS

The authors wish to acknowledge the support provided by the Research, Consultancy and Design Centre (RCDC) of the University of Architecture Civil Engineering and Geodesy – Sofia through Grant No. BN-298/24.

REFERENCES

[1] R. STONELEY (1949) The seismological implications of aelotropy in continental structures. *Royal Astronomical Society Monthly Notices, Geophysical Supplement, London, England* **5** 343-53.

[2] D. BRAMFORD, S. CRAMPIN (1977) Seismic anisotropy – the state of the art. *Geophysical Journal International* **49**(1) 1-8.

[3] S. CRAMPIN, E.M. CHESNOKOV, R.G. HIPKIN (1984) Seismic anisotropy – the state of the art II. *Geophysical Journal of the Royal Astronomical Society* **76**(1) 1-16.

[4] J. LABAKI, E. MESQUITA, R.K.N.D. RAJAPAKSE (2014) Vertical Vibrations of an Elastic Foundation with Arbitrary Embedment within a Transversely Isotropic, Layered Soil. *Computer Modeling in Engineering & Sciences* **103**(5) 281-313.

[5] S. KEAWSAWASVONG, T. SENJUNTICHAI (2021) Vertical Dynamic Response of Rigid Circular Foundation in Multilayered Transversely Isotropic Poroelastic Half-Space. *International Journal of Structural Stability and Dynamics* **21**(9) 2150124.

[6] G. GAZETAS (1981) Strip foundations on cross anisotropic soil layer subjected to static and dynamic loading. *Geotechnique* **31**(2) 161–79.

[7] Y. WANG, R.K.N.D. RAJAPAKSE (1991) Dynamics of rigid strip foundations embedded in orthotropic elastic soils. *Earthquake Engineering & Structural Dynamics* **20**(10) 927–47.

[8] G. CHATZISTEFANOU, G. MANOLIS (2020) BEM-derived impedance functions for 2D inhomogeneous soil media: an engineering practice case study. *Journal of Theoretical and Applied Mechanics, Sofia* **50**(4) 370-388.

[9] C.Y. WANG, J.D. ACHENBACH (1994) Elastodynamic fundamental solutions for anisotropic solids *Geophysical Journal International* **118** 384-392.

[10] F.G. GARCIA-SANCHEZ (2005) "Numerical study of fracture problems in elastic anisotropic and piezoelectric solids". Dissertation. University of Sevilla.

[11] Z. BA, V.W. LEE, J. LIANG, Y. YAN (2017) Scattering of plane qP- and qSV-waves by a canyon in a multi-layered transversely isotropic half-space. *Soil Dynamics and Earthquake Engineering* **98** 120-140.

[12] Z. BA, J. LIANG, V.W. LEE, L. HU (2018) IBEM for Impedance Functions of an Embedded Strip Foundation in a Multi-Layered Transversely Isotropic Half-Space. *Journal of Earthquake Engineering* **22** 1415-46.

[13] Z. BA, J. FU, F. WANG, Y. WANG (2022) Three-Dimensional Dynamic Response Analysis of Rigid Foundation Embedded in Layered Transversely Isotropic Half-Space *Journal of Earthquake Engineering* **26**(16) 8611-28.

[14] S. PARVANOVA, P. DINEVA (2022) Dynamic BEM analysis of elastic foundation on anisotropic half-plane. *Archive of Applied Mechanics* **92** 2617-36.

[15] P. DINEVA, T. RANGELOV (2016) Wave scattering by cracks at macro- and nano-scale in anisotropic plane by boundary integral equation method. *Journal of Theoretical and Applied Mechanics, Sofia* **46**(4) 19-35.

[16] T. RANGELOV, P. DINEVA, D. MANOLISD (2018) Dynamic response of a cracked viscoelastic anisotropic plane using boundary elements and fractional derivatives. *Journal of Theoretical and Applied Mechanics, Sofia* **48**(2) 24-49.

[17] S. PARVANOVA, P. DINEVA (2024) Wave Scattering by Nanoinlcusions in Anisotropic Plane. Part II: Numerical Results. *Journal of Theoretical and Applied Mechanics, Sofia* **54**(2) 201-215.

[18] H.A. PEDERSEN, F.J. SÁNCHEZ-SESMA, M. CAMPILLO (1994) Three-dimensional scattering by two-dimensional topographies. *Bulletin of the Seismological Society of America* **84**(4) 1169-83.

[19] A.A. STAMOS, D.E. BESKOS (1996) 3-D seismic response analysis of long lined tunnels in half-space. *Soil Dynamics and Earthquake Engineering* **15**(2) 111-118.

[20] A.J.B. TADEU, E. KAUSEL (2000) Green's Functions for Two-and-a-Half-Dimensional Elastodynamic Problems. *Journal of Engineering Mechanics* **126**(9) 1093-97.

[21] P. JEAN, C. GUIGOU, M. VILLOT (2004) A 2.5D BEM Model for Ground-Structure Interaction. *Building Acoustics* **11**(3) 157-173.

[22] S. FRANÇOIS, M. SCHEVENELS, P. GALVÍN, G. LOMBAERT, G. DEGRANDE (2010) A 2.5D coupled FE–BE methodology for the dynamic interaction between longitudinally invariant structures and a layered halfspace. *Computer Methods in Applied Mechanics and Engineering* **199**(23-24) 1536-48.

[23] G. RIECKH, W. KREUZER, H. WAUBKE, P. BALAZS (2012) A 2.5D-Fourier-BEM model for vibrations in a tunnel running through layered anisotropic soil. *Engineering Analysis With Boundary Elements* **36**(6) 960-967.

[24] H. LIRAVI, R. ARCOS, D. GHANGALE, B. NOORI, J. ROMEU (2021) A 2.5D coupled FEM-BEM-MFS methodology for longitudinally invariant soil-structure interaction problems. *Computers and Geotechnics* **132** 104009.

[25] H. LI, C. HE, Q. GONG, S. ZHOU, X. LI, C. ZOU (2024) TLM-CFSPML for 3D dynamic responses of a layered transversely isotropic half-space. *Computers and Geotechnics* **168** 106131.

[26] J. BERENGER (1994) A perfectly matched layer for the absorption of electromagnetic waves. *Journal of Computational Physics* **41** 115-135.

[27] U. BASU, A. CHOPRA (2003) Perfectly matched layers for time-harmonic elastodynamics of unbounded domains: theory and finite-element implementation. *Computer Methods in Applied Mechanics and Engineering* **192**(11-12) 1337-1375.

[28] ANSYS: RELEASE 2024.1.1 (2024) Structural Mechanics Package. Canonsburg, Pennsylvania.

[29] S. FRANCOIS, M. SCHEVENELS, G. LOMBAERT, G. DEGRANDE (2012) A two-and-a-half-dimensional displacement-based PML for elastodynamic wave propagation. *Numerical Methods in Engineering* **90**(7) 819-837.

[30] J. DOMINGUEZ (1993) "Boundary Elements in Dynamics". WIT Press/Computational Mechanics Publications Southampton.

[31] M. PAPADOPOULOS, S. FRANÇOIS, G. DEGRANDE, G. LOMBAERT (2018) The influence of uncertain local subsoil conditions on the response of buildings to ground vibration. *Journal of Sound and Vibration* **418** 200-220.

[32] MATLAB. VERSION 23.2.0.2409890 (R2023B) (2023) The MathWorks Inc, Natick, Massachusetts.

[33] J.D. BASS (1995) Elasticity of minerals, glasses, and melts. In: Ahrens, T.J. (Ed.) "Mineral Physics and Crystallography. A Handbook of Physical Constants". AGU Reference Shelf 2. American Geophysical Union, Washington, D.C, pp. 45-63.